



Large anomalous Hall angle accompanying the sign change of anomalous Hall conductance in the topological half-Heusler compound HoPtBi

Jie Chen ^{1,2}, Xing Xu,¹ Hang Li ², Tengyu Guo,¹ Bei Ding,² Peng Chen,¹ Hongwei Zhang,² Xuekui Xi,^{1,2} and Wenhong Wang^{1,2,*}

¹Songshan lake Materials Laboratory, Dongguan, Guangdong 523808, China

²State Key Laboratory for Magnetism, Beijing National Laboratory for Condensed Matter Physics, Institute of Physics, Chinese Academy of Sciences, Beijing 100190, China



(Received 7 February 2021; revised 1 April 2021; accepted 2 April 2021; published 19 April 2021)

Controlling the anomalous Hall effect (AHE) in magnetic topological materials is an important property. Because of the close relationship between anomalous Hall conductance (AHC) and topological band (strong Berry curvature), AHC can be effectively tuned by magnetic field combined with strong spin-orbit interaction and special band structure. In this work, we observed a magnetic field driving the nonmonotonic magnetic field dependence of anomalous Hall resistivity and the sign change in magnetic-field-induced Weyl semimetal HoPtBi. The tunable ranges of the AHC and the anomalous Hall angle are $-75 \sim 73 \Omega^{-1} \text{ cm}^{-1}$ and $-12.3 \sim 9.1\%$, respectively. Anisotropic measurements identified the magnetic field is the key factor in controlling the additional Hall term sign. Further analysis indicated that it originated from the field-induced shift of the Weyl points via exchange splitting of bands near the Fermi level. The large tunable effect of the magnetic field on the electronic band structure provides a path to tune the topological properties in this system. These findings suggest that HoPtBi is a good platform for tuning the Berry phase and AHC with the magnetic field.

DOI: [10.1103/PhysRevB.103.144425](https://doi.org/10.1103/PhysRevB.103.144425)

I. INTRODUCTION

Ternary half-Heusler compounds crystallize in the cubic MgAgAs-type crystal structure. They constitute a large family of materials characterized by various physical and chemical properties [1,2]. Half-Heusler compounds have been intensively studied in the last decades regarding, superconductivity [3–5], giant magnetoresistance [6,7], heavy fermions [8,9], half-metals [10,11], magnetocaloric effect [12], and Seebeck effect [13], because they possess unique multifunctionality that can be easily tuned by small modifications in their composition, morphology or some external factors.

Some pioneering theoretical works [14–16] have recently suggested that rare-earth (*R*)-based half-Heusler compounds (*RTX*), where *T* is a *d*-electron transition metal (Ni, Pd, Pt, ...), and *X* is a pnictogen (Sb, Bi), are promising candidates for topological materials, exhibiting various unconventional physical phenomena, e.g., topological insulators/semimetals [17,18], topological superconductivity [3,19], and spin-wave excitations [20], topologically coupled with the electromagnetic field. All those rare features may emerge in *RTX* phases because of strong Rashba-type spin-orbit interactions, resulting from the lack of inversion symmetry in crystalline systems. The nontrivial topological nature of selected *RTX* compounds has been theoretically predicted using electronic band structure calculations and, after that, experimentally confirmed [21,22].

Among these topological candidates, the magnetic Weyl semimetals attracted growing attention since their large Berry curvature resulted in a strong intrinsic anomalous Hall effect (AHE) when the Weyl nodes were close to the Fermi level [23]. This scenario was well-studied in magnetic topological materials, like $\text{Co}_3\text{Sn}_2\text{S}_2$ [24,25], Co_2MnGa [26], and Fe_3GeTe_2 [27], in which the band crossing points and nodal lines with a topological order host strong Berry curvature [23,28–30]. Therefore, the position of topological bands strongly affects the value and the sign of the anomalous Hall conductance (AHC). In our previous works, we observed the negative magnetoresistance (MR) and extracted the π Berry phase in the rare-earth-based half-Heusler compounds, HoPtBi, which identified the chiral-anomaly-induced negative longitudinal magnetoresistance and confirmed the presence of Weyl fermions [31]. This paper presents a systematic analysis of the experimental results of the temperature- and crystal orientation-dependent AHE in HoPtBi single crystals. Our results reveal a large anisotropic AHE in HoPtBi with the tunable anomalous Hall angles (AHAs) of -12.3 to 9.1% , depending on the geometric configurations of the applied magnetic field (*B*) and electronic current (*I*). This feature is ascribed to the tunable position of Weyl points relative to the Fermi level, which may induce the inversion of Berry curvature. However, more studies in this direction are certainly necessary.

II. EXPERIMENTAL SECTION

HoPtBi single crystals, with a typical size of $1 \times 1 \times 1$ mm, were grown by a solution growth method using a Bi flux [7].

*wenhong.wang@iphy.ac.cn

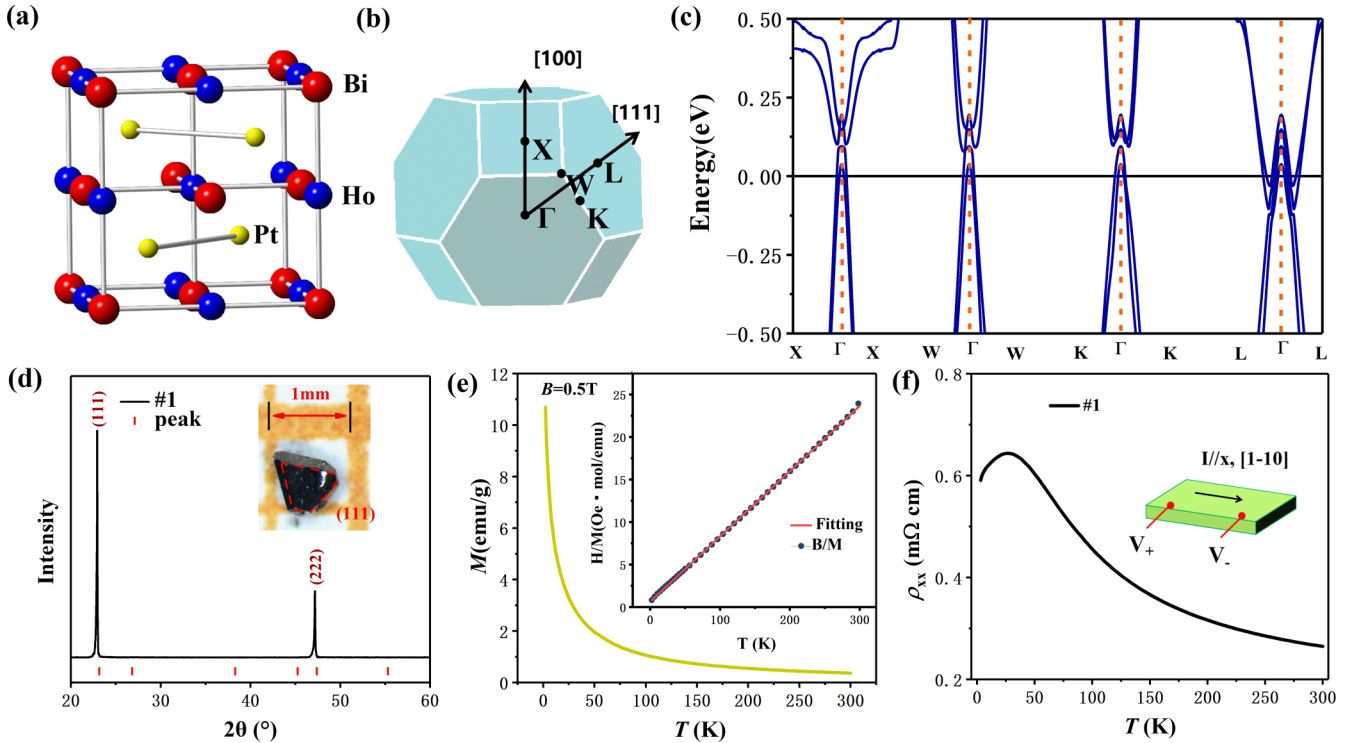


FIG. 1. (a) The crystal structure of HoPtBi with the space group $F-43m$ (216). (b) Brillouin zone and (c) band structure of HoPtBi along the $X-\Gamma-X-W-\Gamma-W-K-\Gamma-K-L-\Gamma-L$ high symmetry line. (d) Single crystal XRD pattern of the (111) plane. The inset is the typical shape of the HoPtBi single crystal. (e) The thermal magnetization of HoPtBi from 2 to 300 K at an external magnetic field $B = 0.05$ T. The inset represents the fitting of the whole paramagnetic region of the thermal magnetization curve by Curie-Weiss law: the extension of the fitting curve intersects the negative x axis, AFM exchange interaction is dominant. (f) Temperature dependence of resistivity curves for sample #1 with current I // $[1-10]$.

The crystal structure was identified using the x-ray diffraction (XRD) method with Cu- $K\alpha$ radiation. The transport and magnetization properties were measured in the physical properties measurement system (PPMS, 9T). The samples were polished into a rectangle shape with a thickness lower than 0.1 mm for transport measurement. A six-probe method was applied to simultaneously measure the magnetoresistance and Hall signals. The misalignment of the electrode was removed by symmetrizing the data between negative and positive magnetic fields. The electronic band structures were calculated using the WIEN2K code, based on the framework of density functional theory [32]. The Perdew-Burke-Ernzerhof generalized gradient approximation [33] was used to calculate exchange correlation potentials. We set the cutoff energy of -6.0 Ry, defining the separation of the valence and core states. Due to heavy elements, we included spin-orbit coupling (SOC) in the calculation. A large exchange parameter, $U_{\text{eff}} = 0.6$ Ry, was applied to Ho.

III. RESULTS

Figure S1 shows a uniform distribution of Ho, Pt, Bi, indicating high-quality HoPtBi single crystals grown by the Bi-flux method [34]. HoPtBi exhibits a cubic MgAgAs-type crystal structure, Fig. 1(a), with a crystal lattice parameter $a = 6.6344$ Å [7]. The corresponding Brillouin zone is shown in Fig. 1(b). The high-symmetry lines $\Gamma-L$ and $\Gamma-X$ represent $[111]$ and $[100]$ crystal planes, respectively. Since the bands

cross the Fermi level around the Γ point, Fig. 1(c) shows the band structure along different high-symmetry lines crossing the Γ point with ferromagnetic states and spin-orbit coupling. The semimetallic band structure is similar to that of other half-Heusler compounds, like GdPtBi [17,35], TbPtBi [22], and YbPtBi [18]. The theoretical calculation of GdPtBi suggested that the direction of magnetic moment significantly influenced the number and position of Weyl points [35]. The magnetic field can easily change the symmetry of the magnetic structure in a paramagnetic material. In theory, besides the strong spin-orbit coupling, the magnetic field can effectively tune the band structure and topological states. Therefore, the tunable effect could be observed in the HoPtBi compound.

The orientation of a single crystal is determined based on the corresponding XRD pattern. As shown in Fig. 1(d), two peaks indicate the (111) crystal plane of sample #1. The inset represents a photograph of the HoPtBi single crystal with the (111) plane making triangle (red dashed line). The thermal magnetization curves are measured from 300 to 2 K under 0.05 T, Fig. 1(e), indicating paramagnetic states in the whole T range. HoPtBi host an antiferromagnetic state in $T < T_N = 1.2$ K [36]. The solid line in the inset is the fitting curve of Curie-Weiss law. The effective magnetic moment $\mu_{\text{eff}} = 10.2 \mu_B$ is closed to the theoretical magnetic moment of $\mu_{\text{Ho}^{3+}} = 10.6 \mu_B$. Figure 1(f) shows the temperature dependence of ρ_{xx} for sample #1 with 0 T and I // $[110]$. The transition of resistivity ρ_{xx} from semiconductor behavior to metallic behavior and small activation energy 18 meV

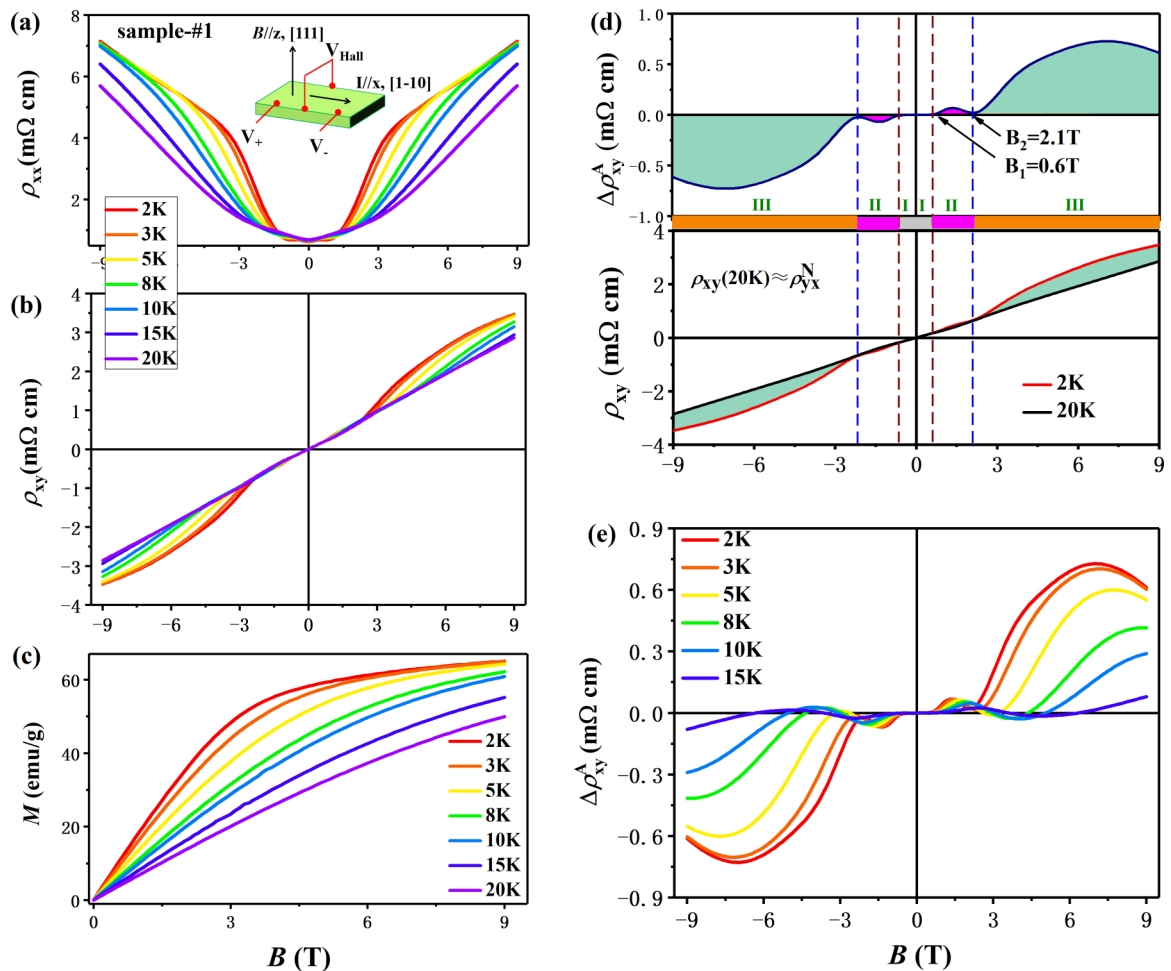


FIG. 2. AHE for sample #1. Magnetoresistance (a) and Hall resistivity (b) for sample #1. The inset of (a) is the configuration of the magnetic field $B//[111]$ and current $I//[1-10]$. (c) Magnetization as a function of B at different T with $B//[111]$. (d) The extracting progress of the anomalous Hall resistivity at 2 K. The lower figure shows Hall resistivity at 2 and 20 K. The upper one shows the additional term $\Delta\rho_{xy}^A$ at 2 K. The total curve can be divided into three regions I, II, and III. The additional term $\Delta\rho_{xy}^A$ at 2 K was obtained by subtracting the linear Hall resistivity at 20 K. (e) The additional term $\Delta\rho_{xy}^A$ for sample #1 at $T < 20$ K.

(Fig. S4) indicates HoPtBi hosts a small gap, which is coincide with band structure.

One of our main finding related to HoPtBi is a large non-monotonic Hall effect. The anomalous behavior in Fig. 2 is explained in sample #1. MR and Hall resistivity of sample #1 are shown in Figs. 2(a) and 2(b), respectively. Compared to B -linear dependence of the normal Hall effect, ρ_{xy} of sample #1 shows an unconventional behavior. The curves deviate from a linear behavior, forming a swell at a high magnetic field, similar to the AHE of TbPtBi [37]. This swell gradually diminishes and shifts to a high magnetic field with the temperature increase, disappearing entirely at $T = 20$ K and $B = 9$ T. The fitting of the normal Hall resistivity indicates that sample #1 shows very high mobility of $5059 \text{ cm}^2 \text{ V}^{-1} \text{ s}^{-1}$, exceeding the maximum value of GdPtBi ($1 \times 10^3 \text{ cm}^2 \text{ V}^{-1} \text{ s}^{-1}$) [38] and TbPtBi ($2.2 \times 10^3 \text{ cm}^2 \text{ V}^{-1} \text{ s}^{-1}$) [39] single crystals. The high quality of the synthesized single crystal also reflects on the magnetoresistance effect. The MR value reaches 1031% at 2 K and 9 T. We also note the complex MR behavior at a low magnetic field, contributing to quantum coherence (weak antilocalization effect and weak localization effect) [7]. Figure 2(c) shows the magnetic field dependence of magne-

tization at low T and $B//[111]$. The Brillouin-function-like behavior induces the magnetization curves saturate at a high magnetic field reaching 60 emu/g at 9 T. In general, Hall resistivity, ρ_{xy} , in magnetic materials can be expressed as follows:

$$\rho_{xy} = R_H B + \rho_{xy}^A, \quad (1)$$

$$\rho_{xy}^A = R_S M, \quad (2)$$

where R_H and R_S are ordinary and anomalous Hall coefficients. ρ_{xy}^A is anomalous Hall resistivity proportional to magnetization in conventional ferromagnetic or ferrimagnetic materials. Apparently, ρ_{xy} of sample #1 is not proportional to magnetization. An additional term, $\Delta\rho_{xy}^A$, with a non-monotonic dependence on M , occurs. Therefore, ρ_{xy} can be expressed as follows:

$$\rho_{xy} = R_H B + \rho_{xy}^A + \Delta\rho_{xy}^A. \quad (3)$$

Since the curves at $B < 0.6$ T and $T < 20$ K almost overlap and the additional term disappears completely at 20 K. Therefore, the additional Hall resistivity $\Delta\rho_{xy}^A$ can be obtained

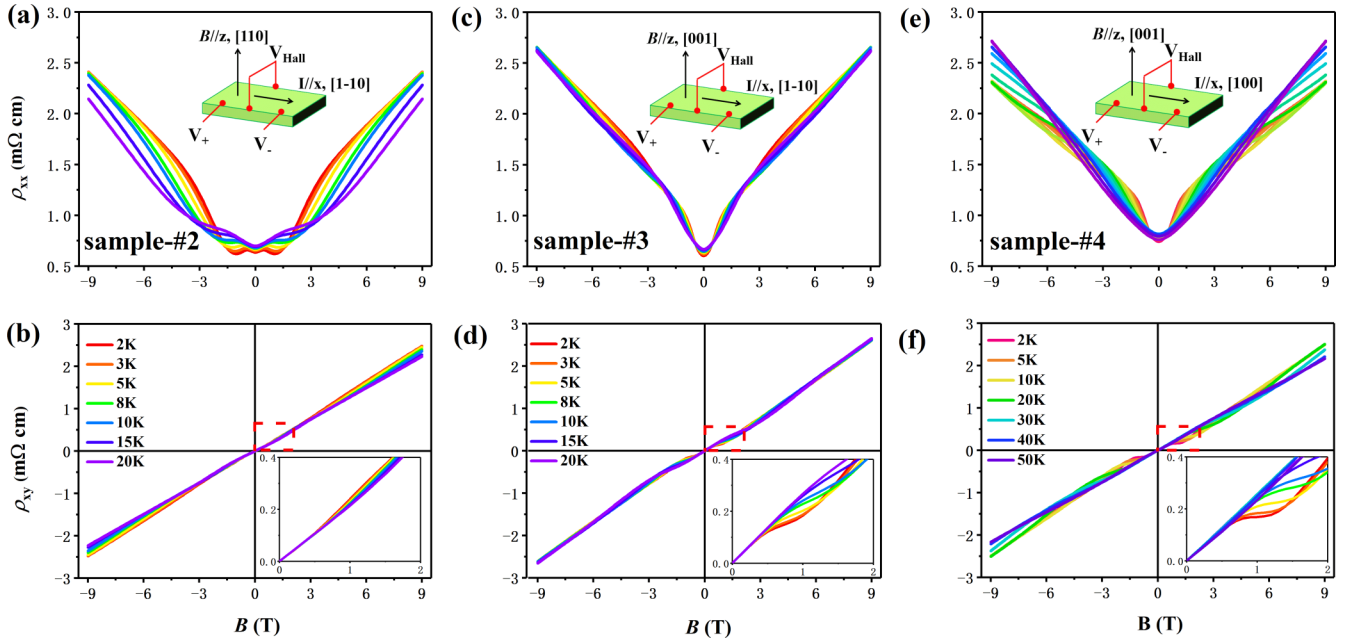


FIG. 3. Hall resistivity ρ_{xy} and magnetoresistance ρ_{xx} at different temperatures for three samples with different configurations of B and I . (a) and (d) are the magnetoresistance ρ_{xx} and Hall resistivity ρ_{xy} , respectively, with $B//[110]$ and $I//[1-10]$. The inset of (b) shows the Hall resistivity at a low magnetic field. (c) and (d) are magnetoresistance ρ_{xx} and Hall resistivity ρ_{xy} for sample #3, respectively, with $B//[001]$ and $I//[1-10]$. (e) and (f) are the results for sample #4 with $B//[001]$ and $I//[100]$.

by subtracting $\rho_{xy}(20\text{ K})$. Figure 2(d) shows the extracted progress of $\Delta\rho_{xy}^A$. The lower figure is Hall resistivity at 2 and 20 K, and the upper figure is the additional Hall resistivity $\Delta\rho_{xy}^A$ at 2 K. According to the $\Delta\rho_{xy}^A$ value, the whole range can be divided into three parts I, II, and III. In part I ($B < 0.6\text{ T}$), $\rho_{xy}(2\text{ K})$ and $\rho_{xy}(20\text{ K})$ show B -linear dependence, indicating that the normal Hall effect dominates the Hall signal. Hence, the extracted $\Delta\rho_{xy}^A$ is almost zero for the overlapping $\rho_{xy}(2\text{ K})$ and $\rho_{xy}(20\text{ K})$ curves. In part II ($0.6\text{ T} < B < 2.1\text{ T}$), the $\rho_{xy}(2\text{ K})$ curve deviates from the linear behavior and forms a small positive swell. The critical magnetic field of AHE is $B_c = 0.6\text{ T}$, which is significantly lower than $B_c = 7\text{ T}$ for TbPtBi [37]. Large magnetic moment and smaller lattice parameter maybe the main factor that HoPtBi have a smaller critical magnetic field. Because the formation of Weyl points in magnetic RPtBi compounds was attributed to an external magnetic-field-induced Zeeman splitting [35]. The magnetic moment of Ho^{3+} ($10.2\mu_B$) is larger than Tb^{3+} ($9.57\mu_B$) and smaller lattice constant may lead to RPtBi need smaller Zeeman energy to form the band crossing (Weyl points). At $B = 2.1\text{ T}$, the $\Delta\rho_{xy}^A$ decreases to almost zero. At this point, the additional signal $\Delta\rho_{xy}^A$ is missing, which is a phenomenon for AHE. In part III ($2.1\text{ T} < B$), another large positive swell appears and extends to fields larger than $B = 9\text{ T}$. The peak of $\Delta\rho_{xy}^A(2\text{ K})$ reaches $0.7037\text{ m}\Omega\text{ cm}$, which is larger than that of GdPtBi ($\Delta\rho_{xy}^A = 0.18\text{ m}\Omega\text{ cm}$) [38] and TbPtBi ($\Delta\rho_{xy}^A = 0.6798\text{ m}\Omega\text{ cm}$) [37]. The extracted $\Delta\rho_{xy}^A$ for sample #1 is shown in Fig. 2(e). With the temperature increase, $\Delta\rho_{xy}^A$ gradually reduces and completely disappears at 20 K, and both of swells are shifting to high magnetic field.

Next, we measured in detail the anisotropic transport properties of this compound. Magnetic field (B) and current (I),

as two main external tunable factors, have a great influence on magnetotransport properties, especially for the Hall effect [40–44]. To clarify the tuning effect of B and I , we designed a series of experiments with different B and I configurations. Besides sample #1, samples #2 and #3 keep the direction of current ($I//[1-10]$) unchanged and rotate B from $[111]$ to $[110]$ and $[001]$. When B turns to the $[110]$ direction (sample #2), ρ_{xx} [Fig. 3(a)] and ρ_{xy} [Fig. 3(a)] show curves similar to sample #1, having lower MR values and smaller swells. However, there is a completely opposite additional Hall signal when B turns to $[001]$. Figure 3(d) shows the negative nonmonotonic magnetic field dependence of Hall signals at a low magnetic field, and the peaks shift to a high magnetic field with temperature increase. The anomalous Hall signal persists up to 50 K and then reverts to a normal Hall effect. Because the current is fixed ($I//[1-10]$), only the magnetic field is changing. We can reasonably deduce that the external magnetic field can effectively tune this nonmonotonic magnetic field dependence of AHE. To identify this fact undoubtedly, we pick another sample with $B//[001]$ and $I//[100]$ (sample #4). Comparing to sample #3, B is fixed, but I changes from $[1-10]$ to $[100]$. The negative nonmonotonic magnetic field dependence of the Hall signal is also observed. It further identifies that the magnetic field but not the current is the key factor of the sign change. The sign change of AHE is another main finding in HoPtBi.

To explore the origin of the anomalous Hall resistivity and the sign change, we discuss the possible origins of $\Delta\rho_{xy}^A$ further. First, $\Delta\rho_{xy}^A$, a nonmonotonic magnetic field dependence, reminds us that a spin texture, such as frustrate magnets and magnetic skyrmion lattices, can provide a fictitious magnetic field and induce a nonproportional Hall effect (topological

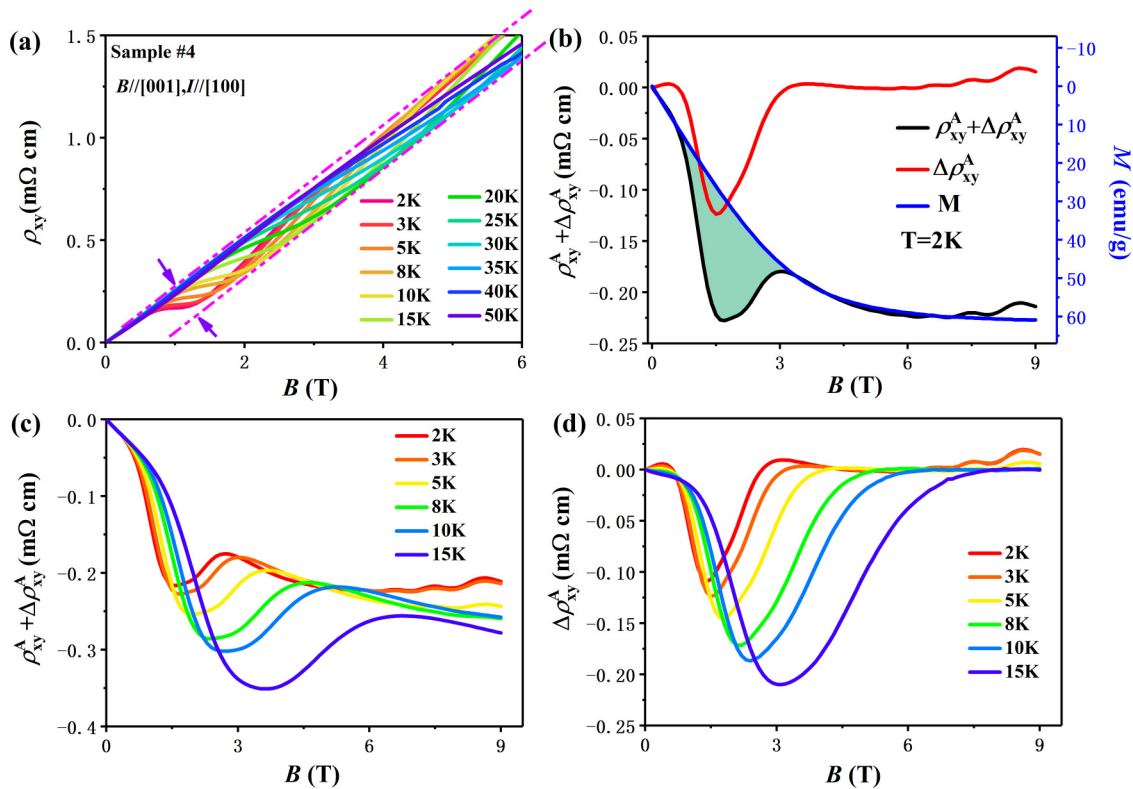


FIG. 4. The extracting progress of the anomalous Hall resistivity for sample #4. (a) Hall resistivity for sample #4 in the 2–50 K range. The dashed lines are a guide for the eye. (b) The anomalous Hall resistivity for sample #4 at $T = 2$ K. (c) The anomalous Hall resistivity contains two terms, ρ_{xy}^A , and additional term, $\Delta\rho_{xy}^A$, $T < 20$ K. (d) The additional term $\Delta\rho_{xy}^A$ for sample #4.

Hall effect) during the magnetization progress [45–49]. In generally, the topological Hall effect usually observed in certain special magnetic materials, such as magnetic skyrmions. However, as shown in Figs. 1(e) and 2, HoPtBi is paramagnetic state in 2–300 K, and topological Hall effect will vanish when magnetization tends toward saturation. It is not coincident with the result in sample #1. Another evidence of excluding topological Hall effect as the origin is that the sign of the topological Hall effect would be determined by the sign of the normal Hall effect [50]. Thus, the sign change of the additional Hall signal in HoPtBi could hardly be reconciled with the constant carrier sign. As shown in Figs. 2 and 3, the slope of the normal Hall resistivities retains a positive sign as the magnetic field changes from [111] to [110] and [001]. Therefore, the sign change of the additional Hall signal dependent on the B direction cannot be explained by the mechanism of the topological Hall effect. The AHE in other rare-earth-based half-Heusler compounds was studied and attributed to the Berry phase of electronic band [18,21,22,35,38,39]. As previously explained, the magnetic field can easily change the symmetry of magnetic structure in paramagnet. The magnetic ordering can tune electronic structure through the strong SOC. Combined with the experimental results that the sign depends on the B direction, the $\Delta\rho_{xy}^A$ sign change should contribute to the change of topological band. We need to point out that the AHE sign change is observed in this family of materials. It also indicates that HoPtBi possesses a more special structure comparing to GdPtBi, TbPtBi, and YbPtBi. The large change

of band structure of HoPtBi is enough to reverse the total Berry curvature.

The Hall resistivities of samples #3 and #4 are different from that of samples #1 and #2. In samples #3 and #4, the term ρ_{xy}^A in Eq. (3), which is proportional to the magnetization, cannot be neglected. Here, we take sample #4 as an example to separate the unconventional Hall effect. In Fig. 4(a), the Hall resistivity forms a negative swell at a medium magnetic field. With temperature increase, the swell peaks shift toward high magnetic fields. The additional Hall term persists to 50 K at 9 T, which is much higher than that of samples #1 and #2. The Fig. 4(b) shows the Hall contribution of ρ_{xy}^A and $\Delta\rho_{xy}^A$ after subtracting the normal Hall ρ_{xy}^N at 2 K for sample #4. The dark line represents the contribution of $\rho_{xy}^A + \Delta\rho_{xy}^A$ and both are negative. The blue line is magnetization M fitting to ρ_{xy}^A . The red line is the additional Hall resistivity, $\Delta\rho_{xy}^A$, mainly distributed in the $0.6 \text{ T} < B < 3 \text{ T}$ region. The critical magnetic field B_c is the same as that of sample #1, identifying that HoPtBi needs a small external magnetic field to form the Weyl states. The $\Delta\rho_{xy}^A$ oscillation in high magnetic field originates from the quantum oscillation which has been reported in our previous result [31]. Figure 3(d) shows the anomalous Hall resistivity at $T < 20$ K for sample #4.

IV. DISCUSSIONS

In Fig. 5, we show the AHC, $\Delta\sigma_{xy}^A$ and the corresponding AHA as a function of T . The $\Delta\sigma_{xy}^A$ and AHA are defined

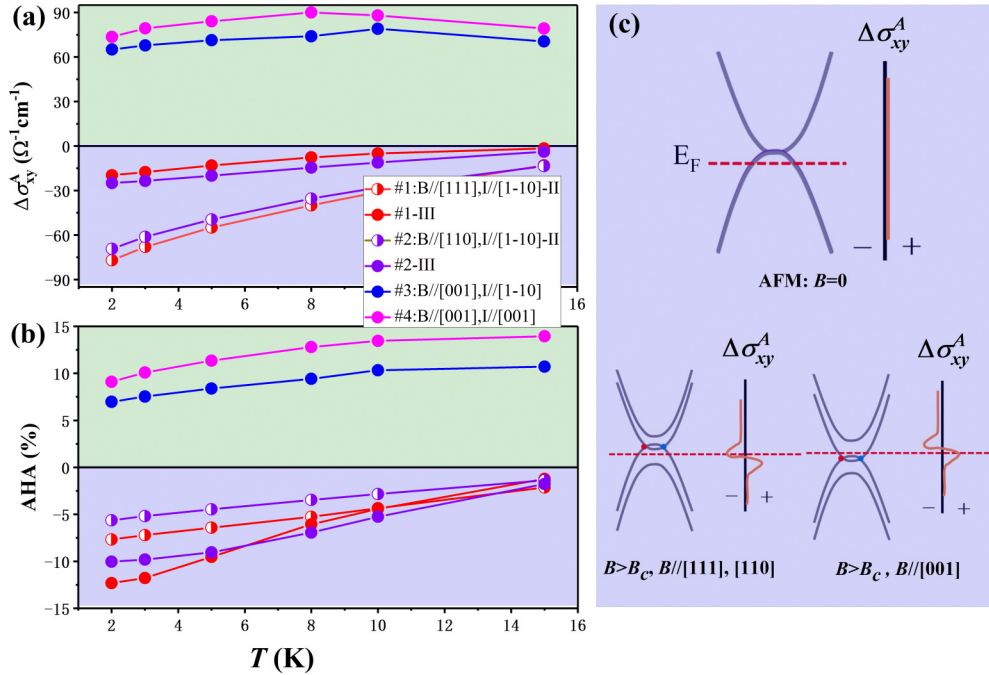


FIG. 5. (a) The additional Hall conductance $\Delta\sigma_{xy}^A$ and (b) the corresponding AHA for samples #1 – #4 at 2 K. All data are obtained from the peak of $\Delta\rho_{xy}^A$. II represents the data gotten from the II region (low magnetic field), and III represents the data from the III region (high magnetic field). (c) The sketches of the mechanism of the AHC and the sign change for HoPtBi. The upper panel: in the absence of an external magnetic field, AHC tends to zero. The lower panel: under various magnetic field directions, the t formed Weyl points shift around E_F and induced the AHC sign change.

as follows: $\Delta\sigma_{xy}^A = -\Delta\rho_{xy}^A/(\rho_{xy}^2 + \rho_{xx}^2)$ and $\text{AHA} = 100 \times \Delta\sigma_{xy}^A/\sigma_{xx}$, respectively. II and III represent that peaks come from the low magnetic field and high magnetic field regions, respectively. $\Delta\sigma_{xy}^A$ for samples #1 and #2 shows negative values and decreases with the temperature. However, for samples #3 and #4, $\Delta\sigma_{xy}^A$ shows positive values and remains almost constant with the temperature. $\Delta\sigma_{xy}^A$ for samples #1-II, #2-II, and samples #3, #4 at 2 K are in the range of $60\text{--}80\ \Omega^{-1}\text{cm}^{-1}$, which is comparable to other half-Heusler compounds [35,38]. In fact, Pavlosiuk *et al.* [36] have observed the anomalous Hall effect in single crystals of HoPtBi. However, the sign change of anomalous Hall resistivity in HoPtBi observed in the current work is rare. On the one hand, we should note that the total Berry curvature change because of the Fermi level (E_F) shifting when the temperature changed from room temperature to low temperatures induced the AHE sign change in SrRuO₃ [29]. On the other hand, La doping of a magnetic oxides EuTiO₃ film also showed an AHE sign change since the electron doping shifted the Fermi level E_F [42]. All these indicate the sign change is closely related to the position of the topological band around E_F .

The giant magneto-band-structure effect whereby a change of magnetization direction significantly modifies the electronic band structure need several criteria, such as magnetically coupled electrons, strong SOC, and a reduced symmetry to maximize SOC anisotropy [51]. Therefore, it is challenging to achieve the AHE sign change in conventional materials using the magnetic field, B , as another factor that may influence the band structure. RPtBi, a rare-earth-based half-Heusler compound with heavy atoms and absence of inversion centers,

was proved to be a magnetic-field-induced Weyl semimetal [17,22,35,52]. Besides, a simple band structure and the crossing point close to E_F make the RPtBi family an ideal platform to control of the Berry phase and AHE by tuning bands with a magnetic field. In Fig. S5, we show the band structures of HoPtBi with magnetic moment parallel to [001], [110], and [111] directions, respectively [34]. The shift crossing point between $M // [001]$ and $M // [110], [111]$ identified the large tunable effect. The chiral anomaly effect and nontrivial Berry phase extracted by Shubnikov–de Haas oscillations in our previous study identified the HoPtBi topological properties [31].

To describe tunable effect and the relationship between the change of the topological band and the sign change of the AHC clearly, we present a simplified schematic diagram in Fig. 5(c). In the absence of magnetic field [antiferromagnetic (AFM) states], the AHC is fixed to zero. Because $4f$ electrons host strong SOC and high electronic tunability, the magnetic field can tune the topological response via rare-earth atoms [35,38]. When the magnetic field is stronger than B_c , the shifting bands induced by the exchange splitting form the Weyl points around E_F . The crossing points shift around the E_F because of the anisotropic tunable effect of magnetic field on the bands, which further leads to the AHC sign change.

V. CONCLUSIONS

In summary, we observed that a magnetic field induced a large anomalous Hall angle and the sign change in magnetic-field-induced Weyl semimetal HoPtBi. The Hall measurements of four samples with different configurations

demonstrated that the magnetic field was the key factor to control the sign of the additional anomalous Hall term. The tunable AHC and AHA ranges reach $-75-73 \Omega^{-1} \text{cm}^{-1}$ and $-12.3-9.1\%$, respectively. Based on the understanding of RPtBi half-Heusler compounds, the Berry phase mechanism was considered as the origin of the nonmonotonic magnetic field dependence of AHE. The results suggested that the sign change of AHE could be ascribed to special band structure and a large tunable effect of external magnetic field on Weyl nodes relative to E_F . Accordingly, the total Berry curvature flipped, and corresponding AHC changed the sign during this progress. The large tunable effect of the magnetic field on the electronic band structures provides a feasible pathway to tune

the topological properties in this system. These results suggest that HoPtBi is a good platform for tuning the Berry phase and AHE with a magnetic field.

ACKNOWLEDGMENTS

This work was supported by the National Science Foundation of China (Grants No. 11974406 and No. 12074415), the Strategic Priority Research Program (B) of the Chinese Academy of Sciences (CAS) (XDB33000000), and China Postdoctoral Science Foundation (Grant No. 3662020M680734).

-
- [1] K. Manna, Y. Sun, L. Muechler, J. Kübler, and C. Felser, *Nat. Rev. Mater.* **3**, 244 (2018).
- [2] F. Casper, T. Graf, S. Chadov, B. Balke, and C. Felser, *Semicond. Sci. Technol.* **27**, 063001 (2012).
- [3] H. Kim, K. Wang, Y. Nakajima, R. Hu, S. Ziemak, P. Syers, L. Wang, H. Hodovanets, J. D. Denlinger, P. M. R. Brydon, D. F. Agterberg, M. A. Tanatar, R. Prozorov, and J. Paglione, *Sci. Adv.* **4**, eaao4513 (2018).
- [4] Y. Nakajima, R. Hu, K. Kirshenbaum, A. Hughes, P. Syers, X. Wang, K. Wang, R. Wang, S. R. Saha, D. Pratt, J. W. Lynn, and J. Paglione, *Sci. Adv.* **1**, e1500242 (2015).
- [5] G. Xu, W. Wang, X. Zhang, Y. Du, E. Liu, S. Wang, G. Wu, Z. Liu, and X. X. Zhang, *Sci. Rep.* **4**, 5709 (2014).
- [6] Z. Hou, W. Wang, G. Xu, X. Zhang, Z. Wei, S. Shen, E. Liu, Y. Yao, Y. Chai, Y. Sun, X. Xi, W. Wang, Z. Liu, G. Wu, and X.-X. Zhang, *Phys. Rev. B* **92**, 235134 (2015).
- [7] J. Chen, H. Li, B. Ding, Z. Hou, E. Liu, X. Xi, G. Wu, and W. Wang, *Appl. Phys. Lett.* **116**, 101902 (2020).
- [8] E. Mun, S. L. Bud'ko, Y. Lee, C. Martin, M. A. Tanatar, R. Prozorov, and P. C. Canfield, *Phys. Rev. B* **92**, 085135 (2015).
- [9] E. D. Mun, S. L. Bud'ko, C. Martin, H. Kim, M. A. Tanatar, J. H. Park, T. Murphy, G. M. Schmiedeshoff, N. Dilley, R. Prozorov, and P. C. Canfield, *Phys. Rev. B* **87**, 075120 (2013).
- [10] M. Baral and A. Chakrabarti, *Phys. Rev. B* **99**, 205136 (2019).
- [11] L. Damewood, B. Busemeyer, M. Shaughnessy, C. Y. Fong, L. H. Yang, and C. Felser, *Phys. Rev. B* **91**, 064409 (2015).
- [12] K. Synoradzki, K. Ciesielski, and D. Kaczorowski, *Acta Phys. Pol. A* **133**, 691 (2018).
- [13] J. Yang, H. Li, T. Wu, W. Zhang, L. Chen, and J. Yang, *Adv. Funct. Mater.* **18**, 2880 (2008).
- [14] H. Lin, L. A. Wray, Y. Xia, S. Xu, S. Jia, R. J. Cava, A. Bansil, and M. Z. Hasan, *Nat. Mater.* **9**, 546 (2010).
- [15] S. Chadov, X. Qi, J. Kubler, G. H. Fecher, C. Felser, and S. C. Zhang, *Nat. Mater.* **9**, 541 (2010).
- [16] D. Xiao, Y. Yao, W. Feng, J. Wen, W. Zhu, X. Q. Chen, G. M. Stocks, and Z. Zhang, *Phys. Rev. Lett.* **105**, 096404 (2010).
- [17] M. Hirschberger, S. Kushwaha, Z. Wang, Q. Gibson, S. Liang, C. A. Belvin, B. A. Bernevig, R. J. Cava, and N. P. Ong, *Nat. Mater.* **15**, 1161 (2016).
- [18] C. Y. Guo, F. Wu, Z. Z. Wu, M. Smidman, C. Cao, A. Bostwick, C. Jozwiak, E. Rotenberg, Y. Liu, F. Steglich, and H. Q. Yuan, *Nat. Commun.* **9**, 4622 (2018).
- [19] H. Xiao, T. Hu, W. Liu, Y. L. Zhu, P. G. Li, G. Mu, J. Su, K. Li, and Z. Q. Mao, *Phys. Rev. B* **97**, 224511 (2018).
- [20] A. S. Sukhanov, Y. A. Onykiienko, R. Bewley, C. Shekhar, C. Felser, and D. S. Inosov, *Phys. Rev. B* **101**, 014417 (2020).
- [21] H. Zhang, Y. L. Zhu, Y. Qiu, W. Tian, H. B. Cao, Z. Q. Mao, and X. Ke, *Phys. Rev. B* **102**, 094424 (2020).
- [22] Y. Zhu, B. Singh, Y. Wang, C.-Y. Huang, W.-C. Chiu, B. Wang, D. Graf, Y. Zhang, H. Lin, J. Sun, A. Bansil, and Z. Mao, *Phys. Rev. B* **101**, 161105(R) (2020).
- [23] A. A. Burkov, *Phys. Rev. Lett.* **113**, 187202 (2014).
- [24] E. Liu, Y. Sun, N. Kumar, L. Muechler, A. Sun, L. Jiao, S.-Y. Yang, D. Liu, A. Liang, Q. Xu, J. Kroder, V. Süß, H. Borrmann, C. Shekhar, Z. Wang, C. Xi, W. Wang, W. Schnelle, S. Wirth, Y. Chen, S. T. B. Goennenwein, and C. Felser, *Nat. Phys.* **14**, 1125 (2018).
- [25] J. Shen, Q. Zeng, S. Zhang, H. Sun, Q. Yao, X. Xi, W. Wang, G. Wu, B. Shen, Q. Liu, and E. Liu, *Adv. Funct. Mater.* **30**, 2000830 (2020).
- [26] A. Sakai, Y. P. Mizuta, A. A. Nugroho, R. Sihombing, T. Koretsune, M.-T. Suzuki, N. Takemori, R. Ishii, D. Nishio-Hamane, R. Arita, P. Goswami, and S. Nakatsuji, *Nat. Phys.* **14**, 1119 (2018).
- [27] K. Kim, J. Seo, E. Lee, K. T. Ko, B. S. Kim, B. G. Jang, J. M. Ok, J. Lee, Y. J. Jo, W. Kang, J. H. Shim, C. Kim, H. W. Yeom, B. Il Min, B. J. Yang, and J. S. Kim, *Nat. Mater.* **17**, 794 (2018).
- [28] D. Xiao, M.-C. Chang, and Q. Niu, *Rev. Mod. Phys.* **82**, 1959 (2010).
- [29] Z. Fang, N. Nagaosa, K. S. Takahashi, A. Asamitsu, R. Mathieu, T. Ogasawara, H. Yamada, M. Kawasaki, Y. Tokura, and K. Terakura, *Science* **302**, 92 (2003).
- [30] F. D. M. Haldane, *Phys. Rev. Lett.* **93**, 206602 (2004).
- [31] J. Chen, H. Li, B. Ding, E. Liu, Y. Yao, G. Wu, and W. Wang, *Appl. Phys. Lett.* **116**, 222403 (2020).
- [32] P. Blaha, K. Schwarz, G. Madsen, D. Kvasnicka, and J. Luitz, *WIEN2K: An Augmented Plane Wave plus Local Orbitals Program for Calculating Crystal Properties* (Vienna University of Technology, Austria, 2001).
- [33] J. P. Perdew, K. Burke, and M. Ernzerhof, *Phys. Rev. Lett.* **77**, 3865 (1996).
- [34] See Supplemental Material at <http://link.aps.org/supplemental/10.1103/PhysRevB.103.144425> for elemental maps, Hall conductance of Samples #3, #5, and #6, fitting of activation energy

- E_g and band structures of HoPtBi with magnetic moment parallel to the [001], [110], and [111] directions.
- [35] C. Shekhar, N. Kumar, V. Grinenko, S. Singh, R. Sarkar, H. Luetkens, S.-C. Wu, Y. Zhang, A. C. Komarek, E. Kampert, Y. Skourski, J. Wosnitzer, W. Schnelle, A. McCollam, U. Zeitler, J. Kübler, B. Yan, H.-H. Klauss, S. S. P. Parkin, and C. Felser, *Proc. Natl. Acad. Sci. USA* **115**, 9140 (2018).
- [36] O. Pavlosiuk, P. Fałat, D. Kaczorowski, and P. Wiśniewski, *APL Mater.* **8**, 111107 (2020).
- [37] J. Chen, H. Li, B. Ding, H. Zhang, E. Liu, and W. Wang, *Appl. Phys. Lett.* **118**, 031901 (2021).
- [38] T. Suzuki, R. Chisnell, A. Devarakonda, Y. T. Liu, W. Feng, D. Xiao, J. W. Lynn, and J. G. Checkelsky, *Nat. Phys.* **12**, 1119 (2016).
- [39] R. Singha, S. Roy, A. Pariari, B. Satpati, and P. Mandal, *Phys. Rev. B* **99**, 035110 (2019).
- [40] J. L. Ma, H. L. Wang, X. L. Wang, and J. H. Zhao, *Phys. Rev. B* **97**, 064402 (2018).
- [41] S. Nakatsuji, N. Kiyohara, and T. Higo, *Nature (London)* **527**, 212 (2015).
- [42] K. S. Takahashi, H. Ishizuka, T. Murata, Q. Y. Wang, Y. Tokura, N. Nagaosa, and M. Kawasak, *Sci. Adv.* **4**, eaar7880 (2018).
- [43] Y. Su and S.-Z. Lin, *Phys. Rev. Lett.* **125**, 226401 (2020).
- [44] H. Polshyn, J. Zhu, M. A. Kumar, Y. Zhang, F. Yang, C. L. Tschirhart, M. Serlin, K. Watanabe, T. Taniguchi, A. H. MacDonald, and A. F. Young, *Nature (London)* **588**, 66 (2020).
- [45] L. Vistoli, W. Wang, A. Sander, Q. Zhu, B. Casals, R. Cichelero, A. Barthélémy, S. Fusil, G. Herranz, S. Valencia, R. Abrudan, E. Weschke, K. Nakazawa, H. Kohno, J. Santamaria, W. Wu, V. Garcia, and M. Bibes, *Nat. Phys.* **15**, 67 (2018).
- [46] Y. Li, N. Kanazawa, X. Z. Yu, A. Tsukazaki, M. Kawasaki, M. Ichikawa, X. F. Jin, F. Kagawa, and Y. Tokura, *Phys. Rev. Lett.* **110**, 117202 (2013).
- [47] B. G. Ueland, C. F. Miclea, Y. Kato, O. Ayala-Valenzuela, R. D. McDonald, R. Okazaki, P. H. Tobash, M. A. Torrez, F. Ronning, R. Movshovich, Z. Fisk, E. D. Bauer, I. Martin, and J. D. Thompson, *Nat. Commun.* **3**, 1067 (2012).
- [48] Q. Qin, L. Liu, W. Lin, X. Shu, Q. Xie, Z. Lim, C. Li, S. He, G. M. Chow, and J. Chen, *Adv. Mater.* **31**, 1807008 (2019).
- [49] T. Kurumaji, T. Nakajima, H. Nakao, S. Sugayama, M. Hirschberger, Y. Taguchi, A. Kikkawa, T.-h. Arima, Y. Yamasaki, H. Sagayama, H. Nakao, Y. Taguchi, T.-h. Arima, and Y. Tokura, *Science* **365**, 914 (2019).
- [50] N. Nagaosa and Y. Tokura, *Nat. Nanotechnol.* **8**, 899 (2013).
- [51] P. Jiang, L. Li, Z. Liao, Y. X. Zhao, and Z. Zhong, *Nano Lett.* **18**, 3844 (2018).
- [52] J. Cano, B. Bradlyn, Z. Wang, M. Hirschberger, N. P. Ong, and B. A. Bernevig, *Phys. Rev. B* **95**, 161306(R) (2017).